Published in final edited form as:
Nat Chem Biol. 2017 July ; 13(7): 745–749. doi:10.1038/nchembio.2375.

A conserved threonine prevents self-intoxication of enoyl-thioester reductases

Raoul G. Rosenthal[1], **Bastian Vögeli**[1], **Tristan Wagner**[2], **Seigo Shima**[2], and **Tobias J. Erb**[1]

[1]Biochemistry and Synthetic Biology of Microbial Metabolism Group, Max Planck Institute for Terrestrial Microbiology, Karl-von-Frisch-Str. 10, D-35043 Marburg, Germany

[2]Microbial Protein Structure Group, Max Planck Institute for Terrestrial Microbiology, Karl-von-Frisch-Str. 10, D-35043 Marburg, Germany

Abstract

Enzymes are highly specific biocatalysts, yet they can perform unwanted side reactions. Here we investigated the factors that direct catalysis in the enoyl-thioester reductase Etr1p. We show that a single conserved threonine is essential in suppressing the formation of a side product that otherwise acts as a high-affinity inhibitor of the enzyme. Substitution of this threonine with isosteric valine increases side product formation by more than six orders of magnitude, while decreasing turnover frequency by only one order of magnitude. Our results show that promoting wanted reactions and suppressing unwanted side reactions are independently operating principles at the active site of Etr1p, and that the active suppression of side reactions is highly conserved in the family of medium chain dehydrogenases/reductases (MDR). Our discovery emphasizes that the active destabilization of competing transition states is an important factor during catalysis, which has implications for the understanding and the de novo-design of enzymes.

Enzymes are known to be highly efficient and highly specific biocatalysts. Yet, many enzymes catalyze intrinsic side activities that give rise to (unwanted) side products despite sustained evolutionary pressure1. One prominent example is the oxygenase side reaction of ribulose-1,5-bisphosphate carboxylase/oxygenase that leads to the fixation of O_2 instead of CO_2, wasting up to 20% of the energy harvested by photosynthesis2. During glycolysis, the cytotoxic compound methylglyoxal is formed as side reaction of triose phosphate

Correspondence and requests for materials should be addressed to T.J.E.

Data availability and additional information. Structural data has been deposited with the Protein Data Bank under accession codes 5LB9 and 5LBX. Any supplementary information and source data is available in the online version of the paper. Reprints and permissions information is available online at http://www.nature.com/reprints/index.html.

Accession codes
Coordinates and structure factors have been deposited with the Protein Data Bank under accession codes 5LB9 (Etr1p T175V variant, monoclinic form) and 5LBX (Etr1p T175V variant, trigonal form).

Author Contributions
R.G.R., B.V. and T.J.E. conceived and designed all experiments, with the exception of crystallography experiments, which were designed together with T.W and S.S. Enzyme kinetic assays and stopped-flow measurements were performed by R.G.R. and B.V. MS experiments were performed by B.V. and R.G.R. and analysed together with N.S. Cortina. Crystallography experiments were performed by B.V. together with T.W. T.W. and B.V. collected the diffraction data and T.W. interpreted the results. R.G.R., B.V. and T.J.E. wrote the paper.

Competing Financial Interests
The authors declare no competing financial interests.

Europe PMC Funders Author Manuscripts

isomerase3–5. Side reactions also occur in terpene synthases that react through highly reactive intermediates, which has raised the question, how in these enzymes the reaction is guided to produce preferentially the desired product against a myriad of different reaction outcomes6. From these examples it becomes apparent that enzyme catalysis is a balance between positive contributions that promote the wanted reactivity along the substrate-to-product reaction coordinate, as well as negative contributions that suppresses unwanted side reactions on the same reaction coordinate7,8. Most research has focused on understanding the principles of positive catalysis, *i.e.*, the active site geometry that leads to stabilization of a productive transition state. Much less, however, is understood about the mechanisms that protect enzymes from performing unwanted side reactions, which have been termed 'negative catalysis'7.

An interesting example with which to investigate these principles are nicotinamide (NAD(P)H)-dependent reductases that are among the most abundant enzymes in biology (16% of all BRENDA entries are NAD(P)H-dependent enzymes)9. NAD(P)H-dependent reductases serve in essential cellular processes, such as energy conservation and fatty acid metabolism10,11. They are important drug targets (*e.g.*, in tuberculosis treatment and hypercholesterolemia therapy12,13, and they are increasingly used in biocatalysis and biotechnology14,15. For more than half a century, NAD(P)H-dependent reductases have been the prime study objects for understanding, inhibiting and engineering cofactor-dependent enzyme catalysis. Only recently, however, has it been realized that mutagenesis can perturb the catalytic cycle of NAD(P)H-dependent reductases and lead to the accumulation of catalytic intermediates and side products9,16.

Mitochondrial enoyl-thioester reductase Etr1p from *Candida tropicalis*17,18 catalyzes the reduction of enoyl-CoAs during fatty acid biosynthesis (Figure 1). Mutation of the active site proton donor, tyrosine 79, to phenylalanine leads to build-up of several covalent adducts between NADPH and the enoyl-thioester substrate crotonyl-CoA16 (Figure 1a). When the Y79F variant is incubated with crotonyl-CoA and NADPH a covalent adduct between the C2-carbon of NADPH and the Cα-carbon of crotonyl-CoA, a "C2-ene adduct", is formed. Note that the purified C2-ene adduct is catalytically competent for the wild type (WT) Etr1p reaction. Etr1p WT effectively converts and protonates the C2-ene adduct, indicating that this adduct lies on (or near to) the reaction coordinate (Figure 1b-c)9. In the Y79F variant, however, that is impaired in protonation, the C2-ene adduct is further converted into another covalent adduct between the C4 carbon of NADPH and the Cα-carbon of crotonyl-CoA, "C4-adduct"16. In contrast to the C2-ene adduct, the C4-adduct acts as competitive inhibitor of Etr1p WT with nanomolar affinity, indicating that it is a dead-end product of the mutated enzyme reaction (Figure 1c). Thus, Etr1p (and putatively other reductases) must have evolved mechanisms to funnel the reaction towards product formation while suppressing formation of the inhibitory C4-adduct.

Here, we show that the large family of MDRs feature a highly conserved threonine residue that almost exclusively serves in suppressing formation of the inhibitory C4-adduct in Etr1p. We demonstrate that the single hydroxyl group of the conserved threonine is essential to maintain a remarkably high suppression of side reactions but has only marginal effects on the catalytic rate of Etr1p. This provides evidence that promoting catalysis and suppressing

side reactions can be independently, co-existing functions at the active site of enzymes. Notably, the threonine residue is more conserved in the MDR enzyme family than residues promoting catalysis, indicating a strong evolutionary pressure on side-reaction suppression in these enzymes. Taken together, our results suggest that the active destabilization of competing transition states, commonly termed as 'negative catalysis', is fundamental to enzyme catalysis and serves as complementary force to transition state stabilization.

Results

A remote T175 contributes to catalysis

To understand which residues contribute to the productive resolution of the C2-ene adduct (positive catalysis) and which prevent formation of C4-adduct ('negative catalysis'), we combined site directed mutagenesis of Etr1p with kinetic isotope effect (KIE) profiling. Our previous studies showed that hydride transfer and protonation become uncoupled when the active site of Etr1p is mutated16. This uncoupling of NAD(P)H consumption and proton transfer makes classical spectrophotometric assays not suited to measure protonation KIEs in Etr1p, and likely in other reductases. For that reason, we established a mass spectrometry based assay that is able to measure the intramolecular KIE on protonation, similar to earlier work by Northrop and coworkers19. The assay quantifies the incorporation ratios of hydrogen versus deuterium from the solvent into the products, which is given as a $^{D}k_{obs}$ (refer to material and methods for details).

With this method we systematically assessed the intramolecular KIE of different Etr1p active site variants on protonation (supplementary results, supplementary Table 1). In a T175V variant, we measured a large intramolecular KIE on protonation ($^{D}k_{obs}$ = 4.8 ± 0.8) compared to the WT (1.8 ± 0.1). This result was surprising considering that T175 is located more than 6 Å away from the Cα of crotonyl-CoA and almost 9 Å away from the Y79 hydroxyl group, the proton donor in Etr1p (supplementary Figure 1). The finding was even more surprising given that S70 and T324 which are in close proximity to Y79 did not show a strong KIE on protonation upon mutation (supplementary Table 1) raising the question how such a remote residue like T175 can affect the protonation step. At the same time, the T175V variant also appeared to be affected in hydride transfer. Compared to the WT, the apparent $^{(NADPH/NADPD)}k_{cat}$ was reduced from 4.3 ± 0.2 in the WT to 0.96 ± 0.04. Reduction of the KIE on hydride transfer to unity in the T175V variant was also remarkable, considering the close proximity of the γ-OH of T175 to the C4 position of the NADPH-nicotinamide ring. In summary, KIE profiling indicated an essential contribution of T175 to catalysis, although the exact role of this active site residue remained unclear.

T175 is not essential to catalysis

Spectrophotometric characterization of T175V with crotonyl-CoA and NADPH showed a consumption of several equivalents of NADPH compared to enzyme during manual mixing time. This very fast initial decrease of NADPH was followed by a slow phase with apparent kinetic parameters of k_{cat} = 0.082 ± 0.005 s^{-1} and a $K_{m\ NADPH}$ of 2.7 ± 0.8 μM, which corresponded to approximately 0.05 % of WT activity. We investigated this unusual NADPH consumption behavior in more detail by stopped flow UV-Vis spectroscopy. In the burst

phase, the initial turnover of T175V was 12 ± 1 s^{-1} at 30 °C, which was 150-fold higher than under steady state conditions, corresponding to 4 % of WT activity under the same conditions (Figure 2a,b). The burst amplitude was directly proportional to the amount of enzyme (supplementary Figure 2) and lasted more than 3 turnovers, indicating that the biphasic behavior was not caused by slow conformational changes of Etr1p T175V or slow product release. Because the initial turnover frequency of T175V was only reduced by one order of magnitude compared to the WT, we concluded that T175 affected the energetics on the substrate-to-product reaction coordinate but was not essential to catalysis.

T175 controls the correct outcome of catalysis

Because results above excluded an essential role of T175 in promoting catalysis, we speculated that the residue might function in funneling intermediates along the reaction coordinate, suppressing the formation of deleterious side products, such as the inhibitory C4-adduct (Figure 1). We thus devised experiments to detect whether the C4-adduct was indeed formed in the T175V variant during catalysis. We used UPLC-MS to screen for C4-adduct formation under steady state conditions. The T175V variant accumulated C4-adduct at an adduct to enzyme ratio of 1.25 ± 0.07 (Figure 2c). C4-adduct formation was independently confirmed by UV-Vis difference scanning (supplementary Figure 3). Notably, we could not detect any C4-adduct formation in the WT with either method, even not in a reaction with 40 mM NADPH, 40 mM crotonyl-CoA, and 15 μM WT (Figure 2c). At a detection limit of 24 nM for the C4-adduct with the UPLC-MS method (defined as detection of the target ion and isotopic pattern in 5 consecutive spectra), WT forms the C4-adduct in less than one in $1.7 \cdot 10^6$ turnovers. In other words, whereas the WT did not show detectable deviations from the substrate-to-product reaction coordinate, almost every third reaction fell off this reaction coordinate in the T175V variant.

To confirm that the observed effects were not due to changes in the secondary or tertiary structure of the variant, we investigated its folding state by circular dichroism (CD). The CD spectrum of T175V was practically superimposable with the WT and all other enzyme variants created in this study, confirming a correct folding state (supplementary Figure 4). To test whether cofactor binding was altered in the T175V variant, we determined the binding affinities of NADPH by isothermal titration calorimetry. T175V showed a binding constant of $1.6 \pm 0.5 \cdot 10^5$ M^{-1} for NADPH, which was comparable to the WT enzyme ($3.8 \pm 1.0 \cdot 10^5$ M^{-1}), and all other variants tested albeit with slower binding kinetics. From these experiments, we concluded that the T175V variant was unaltered in its biophysical properties, and that the observed loss of catalytic control was indeed caused by an altered catalytic behavior.

Structural basis for loss of catalytic control in T175V

To understand the structural base for the loss of catalytic control in T175V compared to WT we crystallized T175V. The structure confirmed a correct folding of the enzyme. The active site including the water network of apo-WT (PDB: 4W99 at 2.0 Å) and T175V (PDB: 5LB9 at 2.1 Å monoclinic crystals and 5LBX at 2.5 Å trigonal crystals) were superimposable with a root-mean-square deviation of 0.44 Å for all Cα atoms. There was one notable exception. A water molecule in direct contact with T175 was shifted by 1 Å in the T175V variant

compared to the WT (supplementary Figure 5). We note that in contrast to earlier assumptions20,21, this specific change in the water network did not cause a collapse of the apoenzyme's active site.

The tertiary complex of T175V occupied by $NADP^+$ and crotonyl-CoA also showed a WT-like active site geometry with a root-mean-square deviation of 0.49 Å for all Cα atoms compared to tertiary WT complex (PDB: 4WAS). The small movement of the water molecule observed in the apo-form of T175V translated to a tilt of the nicotinamide ring by 17.5° in the tertiary complex of T175V compared to the WT (Figure 3, supplementary Figure 6 and 7). This tilt was observed in monoclinic and trigonal crystals of T175V (supplementary Figure 8), ruling out a crystal packing artifact. The tilt of the nicotinamide caused a 1 Å shift of the nicotinamide-C4 towards the Cα of crotonyl-CoA in T175V. This small difference seems to form the basis for the remarkable loss of discrimination against C4-adduct formation in the T175V variant by more than 106 compared to the WT.

Catalytic control is highly conserved in the MDR family

Interestingly, C4-adducts are already known to be potent inhibitors of NAD(P)H-dependent enzymes. A C4-adduct of lactate and NAD^+ was reported to inhibit lactate dehydrogenase22, the C4-adduct of NAD^+ and 3-pentanone was described to act as inhibitor of *Drosophilla melanogaster* alcohol dehydrogenase23, and the C4-adduct of finasteride (a steroid analog) and NADH inhibits human 5α-reductase, which is used to treat benign prostatic hyperplasia and male pattern baldness24. This inhibitory potential of C4-adducts postulates a strong evolutionary driving force to suppress their formation of during catalysis, which is reflected in the fact that T175V is one of the most conserved residues in the MDR superfamily (supplementary Figure 9).

Moreover, the high grade of conservation of T175 in the MDR superfamily suggests that suppressing off-pathways on the substrate-to-product reaction coordinate seems to be a stronger evolutionary constraint than lowering the energetics of the reaction coordinate itself. While the electrophilic donor in different members of the MDR superfamily can be ***1)*** a proton donor, such as tyrosine (Etr1p), lysine or aspartate (human FAS25 and polyketide synthase enoyl-reductase domains9,26), ***2)*** a CO_2 co-substrate (Ccr)27,28, or ***3)*** might even lack an active site electrophile (LovC)29, a homologue of T175 is strongly conserved in all these enzymes. This indicates that the role of T175 in preventing C4-adduct formation is essential across the entire MDR enzyme family. We tested this hypothesis by introducing an analogous T195V mutation into crotonyl-CoA carboxylase/reductase (Ccr), a CO_2-fixing member of the MDR superfamily30. This also resulted in the formation of the C4-adduct during catalysis (supplementary Figure 10).

We noted that the C4-adduct is a diffusible compound that once formed is not limited to self-intoxicate the enzyme that formed it, but could also inhibit other enzymes with overlapping substrate specificities. Such postulated cross-inhibition would have direct implications for the evolutionary pressure to avoid C4-adduct formation could act beyond the individual enzyme level. We tested this hypothesis with two different members of the MDR superfamily that catalyze completely different reactions, the enoyl-CoA reductase Etr1p, and above mentioned reductive enoyl-CoA carboxylase Ccr30. Etr1p WT was practically

inactive in reactions mixtures of Ccr T195V with NADPH and crotonyl-CoA indicating an effective cross inhibition between the two enzymes (Figure 4). This finding strongly suggests that guiding substrates effectively along the reaction coordinate by suppressing deleterious side reactions is a complementary evolutionary force to transition-state-stabilization, which is as fundamental to enzyme evolution as the latter one.

Discussion

Previous publications on enzymes from the MDR family speculated that T175 might be important for puckering of the nicotinamide ring during catalysis20. Here, we provide a surprising alternative explanation according to which this residue has specifically evolved to protect Etr1p and other NAD(P)H-dependent reductases from intoxication through formation of a deleterious side product of the enzymatic reaction. T175 does not promote catalysis, but serves almost exclusively in controlling the catalytic outcome of the enzyme reaction. This is reflected by the fact that the turnover frequency of T175V remains essentially unchanged, while the error rate of the reaction is increased by more than six orders of magnitude in the same variant. The reason for this dramatic loss of catalytic control apparently lies in surprisingly subtle changes in the geometry structure of the active site. Our results indicate that the hydroxyl group of T175 alone is responsible for guiding the enzyme reaction with high precision. To our knowledge there is no current example –and no simple explanation– of how a single hydroxyl group could have such a strong effect on the catalytic outcome of a reaction.

On a more general note, our results demonstrate that the active site of enzymes can feature catalytic residues of distinct functionality. Residues such as Y79 that promote catalysis, and residues such as T175 that control the catalytic outcome of a given enzyme by actively suppressing unwanted side reactions. Although the existence of active site residues that guide enzyme reactions has been proposed more than 25 years ago7, the discovery that T175 almost exclusively serves such a function is to our knowledge the first direct experimental evidence of this hypothesis.

Our finding that residues promoting enzyme reactions (positive catalysis) and residues directing enzyme reactions (‘negative catalysis’) can function relatively independent from each other at the active site challenges the common understanding of enzyme catalysis, according to which these two traits are inherently linked with each other. For coenzyme B12-dependent methylmalonyl-CoA mutase it was shown that an arginine is essential in suppressing an inactivating side reaction31. However, mutation of this arginine also affected k_{cat} by a factor of 10^4. Another example are pyridoxal phosphate (PLP) dependent enzymes, which catalyze very different reactions that all originate from a common reaction intermediate. It is generally assumed that reaction selectivity in these enzymes is maintained through promoting catalysis by stabilization of the favored transition state and/or destabilization of the ground state of the favored reaction intermediates32,33.

In contrast, our results suggest that binding and promoting productive transition states during catalysis is not necessarily sufficient when close, competing transition states can lead to deleterious side products. It seems almost a logical consequence that in such cases side

reactions need to be actively suppressed by the destabilization of competing transition states to give rise to a proficient enzyme. In this light, the function of active site residues that are conserved but not known to be essential for catalysis so far might require a closer (re-)inspection. An example are histidine 257 and phenylalanine 200 in human purine nucleoside phosphorylase. Mutation of these residues to glycine affects catalytic activity by 20- to 40-fold, but increase an N3-inosine isomerization side-reaction by at least 125- to 250-fold over the level of detection, indicating a potential role in 'negative catalysis' for these residues34. However, even for active site residues that are apparently essential for catalysis, it remains to be tested, whether they confer a positive catalytic function or if they prevent accumulation of inhibitory side-products like in case of Etr1p.

Taken together, our results emphasize that enzyme catalysis needs to be understood as combination of positive and negative constraints on the substrate-to-product reaction coordinate. We expect that these findings will (*i*) lead to a reinvestigation of the principles operating during enzymatic catalysis, (*ii*) clarify the role of many conserved active site residues for which no apparent function could be assigned, so far, and (*iii*) be of high relevance for rational enzyme design. Similar to the concept of 'negative design' already used in the de novo design of proteins31, including 'negative catalysis' elements as a basic design constraint could pave the way to new efficient and precise catalysts in biology and chemistry.

Material and Methods

Chemicals

$NADP^+$ and NADPH (as sodium salts) were purchased from Roth AG, crotonic anhydride were purchased from Sigma Aldrich AG, coenzyme A from Roche Diagnostics. Crotonyl-CoA and C2-ene adduct were synthesized and purified as reported earlier8. All salts and solvents were of analytical grade.

(4*R*)-[4-$^2H_1$]NADPH synthesis

(4*R*)-[4-$^2H_1$]NADPH was synthesized according to previously published protocols28. Synthesis products were confirmed by analytical HPLC and comparison to analytical standards of NADPH. The deuterium incorporation into (4*R*)-[4-$^2H_1$]NADPH was confirmed to be >95% by mass spectrometry. (4*R*)-[4-$^2H_1$]NADPH was dissolved in 0.5 mM NaOH (aq) after lyophilization and stored at -80 °C until it was used.

Cloning and mutagenesis

The plasmid containing Etr1p WT and Ccr were constructed in previous studies. Plasmids carrying desired point mutations were generated using the QuikChange® Site-Directed Mutagenesis with 60 ng of template plasmid, Phusion® DNA polymerase (Thermo Scientific™) and the primers listed in supplementary Table 2. The resulting mutated plasmids were confirmed by sequencing (Eurofins AG, Germany). Plasmids carrying the correct mutations were transformed into *E.coli* BL21(DE3) (Invitrogen ™) for protein expression.

Protein expression and purification

Etr1p and variants were expressed according to previously described protocols9 and desalted into 150 mM NaCl, 20 mM TrisHCl at pH 7.9 (at room temperature) unless otherwise stated. Ccr Wt and T195V was expressed according to previously described methods9 and desalted into the same buffer as Etr1p and variants. Protein concentrations were determined with a Thermo Scientific™ NanoDrop 2000 and extinction coefficients calculated with the ExPASy server (PMID: 10027275).

Stopped flow spectroscopy

Measurements were recorded on a thermo-stated stopped flow unit (SFM-20 connected to a MOS-200, equipped with a Xe(Hg)-lamp and a TC-100/10 cuvette, Bio-Logic Science Instruments SAS, Claix, France) set to 30 °C. Syringe 1 contained 320 μM NADPH and 240 μM crotonyl-CoA in 20 mM Tris-HCl, 150 mM NaCl buffer pH 7.9 and syringe 2 contained 5.0 μM of Etr1p WT or T175V in the same buffer. Data were collected at 340 nm every 1 ms for the first 0.3 s, every 500 ms till 10 s and every 1 s up to a total of 600 s. To estimate initial turnover rates of Etr1p and its variants, the quasi-linear phase of the curve in the first 10 ms was fitted with linear regression to give a lower estimate for the initial rate constant.

Mass spectrometry

Kinetic isotope effects on protonation were measured with ultra-performance liquid chromatography-high resolution heated electrospray ionization mass spectrometry (UPLC HR HESI-MS) analysis a Q-Exactive Plus™ mass spectrometer (ThermoFisher Scientific, San Jose, CA, USA) connected to a Ultimate 3000 (Dionex, Sunnyvale, CA, USA) UPLC system.

Isothermal calorimetry

Proteins were purified as described above and concentrated to about 100 μM (±10 μM). The final concentration was determined in quadruplicate as described above and this value was used for further calculations. The ITC cell of a VP-ITC (GE Healthcare) was loaded with 220 μl of a degassed protein solution and the syringe was filled with a 1.5 mM degassed NADPH solution (the concentration was determined by the absorption at 340 nm with a Thermo Scientific™ NanoDrop 2000 using $\varepsilon_{340\ nm\ NADPH} = 6.2\ cm^{-1}\ mM^{-1}$) in the same buffer (150 mM NaCl, 20 mM TrisHCl at pH 7.9). The titration was spread over 20 injections with one initial dummy injection. The values association constants were determined in duplicate.

KIE on protonation

Reactions for the measurement of kinetic isotope effect on protonation in Etr1p WT and variants contained 100 mM Na_2HPO_4 (pH 7.9), 0.25 mM NADPH, 1.25 μM crotonyl-CoA, and a variable amount of D_2O to give the desired percentage of D_2O, between 7 and 80 %. The enzyme was equilibrated with the deuterated buffer for at least 120 min (to allow for hydrogen exchange with the buffer) before the addition of the last substrate, crotonyl-CoA, from a stock solution of 187.5 μM (to a final volume of 150 μL). Variant enzymes were added at 125 nM and the WT at 25 nM final concentration. Reactions were incubated at

room temperature for 1 hour before diluting 10 times with 25 mM ammonium formate with 2% MeOH (pH 3.5) prior to analysis. Samples were analyzed with ultra-performance liquid chromatography-high resolution heated electrospray ionization mass spectrometry (UPLC HR HESI-MS) analysis on a Q-Exactive Plus™ mass spectrometer (ThermoFisher Scientific™, San Jose, CA, USA) connected to a Ultimate 3000 (Dionex™, Sunnyvale, CA, USA) UPLC system. Chromatographic separation prior to mass analysis was done with a Kinetex® 1,7 µm XB C-18 100 Å, 50 x 2.1 mm column (Phenomenex®, Torrance, CA, USA). Injection volume was 5 µL. Reaction products were separated using a mobile phase system comprised of 25 mM ammonium formate pH 8.1 (A) and methanol (B). Chromatographic separation was carried out using the following gradient condition at a flow rate of 0.55 mL min^{-1}: 0 min, 5%; 1.5 min, 5%; 6.5 min, 95%; 7.5 min, 95%; 7.7 min, 5%; 10.5 min 5%. The $[butyryl\text{-}CoA + H]^+$ mother ion was isolated (840 ± 3.5 m/z) and fragmented with argon at 25 eV. The isotopic pattern on the $[butyryl\text{-}pantothenate + H]^+$ fragment-ion (331.150 m/z) was measured to determine the deuterium incorporation content.

The kinetic isotope effect on protonation, $^{D}k_{obs}$, was determined by fitting the dependence of the ratio of product, butyryl-CoA, with an incorporated deuterium ($product_D$) to product with an incorporated hydrogen ($product_H$) versus the ratio of D_2O (f_{D2O}) to H_2O ($1\text{-}f_{D2O}$) in the buffer with the following equation:

$$\frac{product_D}{product_H} = {}^{D}k_{obs} \cdot \frac{f_{D2O}}{1 - f_{D2O}}$$

The $product_H/product_D$ ratio was calculated by comparing the isotopologue distributions of different samples against a sample with a natural abundance isotopologue distribution as reference. The $product_D/product_H$ ratio of a sample was the calculated with the following equation from the integrated traces of the specific ions:

$$\frac{product_D}{product_H} = \frac{[M+1] - [M+0] \cdot \left(\frac{[M+1]}{[M+0]}\right)}{[M+0]}$$

[M+0] and [M+1] represent the integrals of the [M+0] and [M+1] peaks and ([M+1]/[M+0]) reference represents the ratio of [M+0]/[M+1] in the reference sample with a natural abundance isotopologue distribution.

All data was analyzed with idms_quan-0.0.9-py2-none-any.whl package (www.emzed.ethz.ch) that was especially developed to standardize and automatize the data analysis of kinetic isotope data with EmZed32 using the equations specified above. Measurements were performed in duplicate.

Detection of C4-adduct

To a reaction mixture of 1 µl 500 mM Na_2HPO_4 (pH 7.9), 1 µl 200 mM NADPH and 1 µl 200 mM crotonyl-CoA; 1 µl 60 µM ($3.7 \cdot 10^{-4}$ equivalents) of Etr1p WT or T175V (in 150 mM NaCl, 20 mM TrisHCl pH 7.9) was added. The assays for Ccr WT and Ccr T195V contained 1 µl of 30 mM enzyme, 1 µl 60 µM crotonic anhydrase and additionally 1µL of

200 mM $KHCO_3$. The assay was reacted for 2 minutes on ice before being quenched with 4 µl acetonitrile and immediately injected for analysis.

The calibration curve for the C4-adduct was made with a dilution series made with pure C4-adduct isolated as previously described16. A stock of 12 µM of C4-adduct was made by dissolving the lyophilized C4-adduct into 100 mM Na_2HPO_4 (pH 7.9). This stock was diluted to 3.0 µM, 0.60 µM, 0.125 µM and 0.025 µM and dilutions were kept on liquid nitrogen till between diluting and injecting into the UPLC-MS. C4-adduct eluted at 3.1 min with the employed gradient (see below). The extracted ion chromatogram of m/z = 791.123 ± 0.005 (calc. mass m/z =791.1235, the mass difference of 1ppm is within the mass accuracy of the MS) was smoothed with the default algorithm (Gaussian) of MassHunter Qualitative Analysis software (Agilent Technologies Inc. Santa Clara, CA, USA).

Samples were measured on a 6550 iFunnel Q-TOF mass spectrometer (Agilent Technologies Inc. Santa Clara, CA, USA) equipped with an electrospray ionization source set to positive ionization mode through a 1290 Infinity UPLC (Agilent Technologies Inc. Santa Clara, CA, USA). Chromatographic separation was carried out on a RP-18 column (50 mm x 2.1 mm, particle size 1.7 µm, Kinetex XB-C18, Phenomenex) using a mobile phase system comprised of 50 mM ammonium formate pH 8.1 (A) and methanol (B) with following gradient at a flow rate of 250 µl/min: 0 min 0% B; 1 min 0% B, 6 min 80% B; 8 min 80% B; 8.5 min 0 %B.

Capillary voltage was set at 3.5 kV and nitrogen gas was used as nebulizing (20 psig), drying (13 l/min, 225 °C) and sheath gas (12 l/min, 350 °C). MS data were acquired with a scan range of 500-1200 m/z. Targeted MS/MS was carried out on 791 m/z (z=2) with an isolation width of approximately 4 m/z and a collision energy of 20 eV with an acquisition time of 1000 ms/spectrum.

LC-MS and LC-MS/MS data were analyzed using MassHunter Qualitative Analysis software (Agilent Technologies).

Spectrophotometric enzyme assays

Assays were carried out on a Carry-60 UV/Vis spectrometer (Agilent Technologies Inc. Santa Clara, CA, USA) at 30 °C using quartz cuvettes (10-mm path-length; Hellma® (Germany)). All assays were carried out in 100 mM Na_2HPO_4, pH 7.9. For determination of the kinetic parameters starting from NADPH and crotonyl-CoA assays contained 200 µM crotonyl-CoA and were started by adding enzyme to the following end concentrations: 3 nM Etr1p WT, 5 nM Etr1p S70A, 5 nM Etr1p T324A, 10 nM Etr1p S70A T324A, 6.8 µM Etr1p Y79F or $1.1 \cdot 10^2$ nM Etr1p T175V. Kinetic parameters were determined by varying the NADPH or (4*R*)-[4-$^2H_1$]NADPH concentration (between 1 and 64 µM) and following disappearance of NADPH at 340 nm using an absorption coefficient of $\varepsilon_{340\ nm} = 6.2\ cm^{-1}\ mM^{-1}$ 35. For each concentration chosen, at least triplicate measurements were performed. For Etr1p Y79F $\Delta\varepsilon_{340}$ nm = 2.5 $cm^{-1}\ mM^{-1}$ ($\varepsilon_{340\ nm\ NADPH} = 6.2\ cm^{-1}\ mM^{-1}$, $\Delta\varepsilon_{340\ nm\ C4\text{-}adduct} = 3.7\ cm^{-1}\ mM^{-1}$ was used. Assays for determination of kinetic parameters on C2-ene adduct were by directly adding lyophilized, purified C2-ene adduct and following its disappearance at 370 nm using an extinction coefficient of $\varepsilon_{370\ nm} = 6.9\ cm^{-1}\ mM^{-1}$ 9.

Kinetic parameters with the C2-ene adduct were determined from at least 18 independent measurements at varying concentrations. The KIEs on hydride transfer were calculated from $^{H}k_{cat}/^{D}k_{cat}$ and $(^{H}k_{cat} \cdot K_{m\ D})/(^{D}K_{cat} \cdot K_{m\ H})$ ratios. For all kinetic parameters determined, the corresponding errors are given as 95% confidence intervals.

Cross inhibition of Ccr T195V and Etr1p WT

To investigate whether the C4-adducts formed in Ccr T195V could inhibit Etr1p WT, a reaction with 200 μM NADPH and 200 μM crotonyl-CoA in 100 mM Na_2HPO_4 (pH 7.9) was started by 1 volume percent of either 0.5 μM Ccr WT stock 170 μM Ccr T195V stock. The reaction was allowed to develop for 30 s before adding 1 volume percent of a 50 μM Etr1p WT stock.

Protein crystallization

The purified enzymes were crystallized in sitting drops. Etr1p was crystallized at 15 mg/mL with 5 mM NADP and 5 mM of crotonyl-CoA in the gel filtration buffer (100 mM NaCl, 20 mM TrisHCl pH 7.9). In most experiments, 1 μl of enzyme solution and 1 μl of reservoir solution were mixed in the wells of a crystallization plate (CombiClover Junior Plate, Jena Bioscience). Two different crystalline forms appeared after one week at 25°C. Cubic crystal belonging to the trigonal form appears in 2.0 M $(NH_4)_2SO_4$, 100 mM N-(2-acetamido)-2-iminodiacetic acid (ADA)/NaOH (pH 6.4). Rod shape crystal belonging to the monoclinic form appears in 1.85 M $(NH_4)_2SO_4$, 100 mM ADA pH 6.4 using streak seeding to enhance crystals size. Crystals were immersed in a solution containing 30% (v/v) glycerol, 2.0 M $(NH_4)_2SO_4$, 100 mM ADA pH 6.4 prior to freezing in liquid nitrogen to prevent water-crystal formation.

Structural analysis

Data were collected at the X10SA beamline from the Swiss Light Synchrotron (Villigen) on a Pilatus 6M (Dectris AG, Switzerland). Datasets were processed with XDS36 and scaled with SCALA from the ccp4 suite37. Both crystal structures were solved by molecular replacement with Phaser from PHENIX package38 using the PDB: 4WAS as a template. The starting models for molecular replacement were first refined with REFMAC539. All models were then manually rebuilt with COOT40 and further refined with PHENIX38. For both structure restraints for non-crystallographic symmetry (NCS) and a translation–liberation–screw-rotation (TLS) were applied. Final models were validated through the MolProbity server41 (http://molprobity.biochem.duke.edu). Data collection and refinement statistics are reported in Supplementary Table 3. Figures were generated and rendered with PyMOL (Schrödinger, LLC). The standard deviations between the structures were calculated with the Superpose program of the ccp4 suite.

Supplementary Material

Refer to Web version on PubMed Central for supplementary material.

Acknowledgments

The authors thank R. Lill and U. Mühlenhoff at the Core facility Protein spectroscopy and protein biochemistry of the University of Marburg for providing access to the stopped flow instrument and N. S.Cortina for high resolution mass spectrometric analyses. This work was supported by the Max Planck Society and the European Research Council (ERC 637675 'SYBORG'; granted to T.J.E.).

References

1. Khersonsky O, Tawfik DS. Enzyme Promiscuity: A Mechanistic and Evolutionary Perspective. Annual Review of Biochemistry. 2010; 79:471–505.
2. Zhu XG, Long SP, Ort DR. What is the maximum efficiency with which photosynthesis can convert solar energy into biomass? Current Opinion in Biotechnology. 2008; 19:153–159. [PubMed: 18374559]
3. Browne CA, et al. Studies of the histidine residues of triose phosphate isomerase by proton magnetic resonance and x-ray crystallography. J Mol Biol. 1976; 100:319–43. [PubMed: 3655]
4. Richard JP. Kinetic parameters for the elimination reaction catalyzed by triosephosphate isomerase and an estimation of the reaction's physiological significance. Biochemistry. 1991; 30:4581–5. [PubMed: 2021650]
5. Iyengar R, Rose IA. Concentration of activated intermediates of the fructose-1,6-bisphosphate aldolase and triosephosphate isomerase reactions. Biochemistry. 1981; 20:1223–9. [PubMed: 7013790]
6. Major DT, Freud Y, Weitman M. Catalytic control in terpenoid cyclases: multiscale modeling of thermodynamic, kinetic, and dynamic effects. Current Opinion in Chemical Biology. 2014; 21:25–33. [PubMed: 24735749]
7. Retey J. Enzymatic-Reaction Selectivity by Negative Catalysis or How Do Enzymes Deal with Highly Reactive Intermediates. Angewandte Chemie-International Edition in English. 1990; 29:355–361.
8. Bar-Even A, Milo R, Noor E, Tawfik DS. The Moderately Efficient Enzyme: Futile Encounters and Enzyme Floppiness. Biochemistry. 2015; 54:4969–4977. [PubMed: 26219075]
9. Rosenthal RG, et al. Direct evidence for a covalent ene adduct intermediate in NAD(P)H-dependent enzymes. Nature Chemical Biology. 2014; 10:50–U85. [PubMed: 24240506]
10. Saraste M. Oxidative phosphorylation at the fin de siecle. Science. 1999; 283:1488–1493. [PubMed: 10066163]
11. Harwood JL. Fatty-Acid Metabolism. Annual Review of Plant Physiology and Plant Molecular Biology. 1988; 39:101–138.
12. Quemard A, et al. Enzymatic Characterization of the Target for Isoniazid in Mycobacterium-Tuberculosis. Biochemistry. 1995; 34:8235–8241. [PubMed: 7599116]
13. Stewart MJ, Parikh S, Xiao GP, Tonge PJ, Kisker C. Structural basis and mechanism of enoyl reductase inhibition by triclosan. Journal of Molecular Biology. 1999; 290:859–865. [PubMed: 10398587]
14. Schmid A, et al. Industrial biocatalysis today and tomorrow. Nature. 2001; 409:258–268. [PubMed: 11196655]
15. Mansell DJ, et al. Biocatalytic Asymmetric Alkene Reduction: Crystal Structure and Characterization of a Double Bond Reductase from Nicotiana tabacum. ACS Catal. 2013; 3:370–379. [PubMed: 27547488]
16. Rosenthal RG, et al. The use of ene adducts to study and engineer enoyl-thioester reductases. Nature Chemical Biology. 2015; 11:398–400. [PubMed: 25867044]
17. Airenne TT, et al. Structure-function analysis of enoyl thioester reductase involved in mitochondrial maintenance. Journal of Molecular Biology. 2003; 327:47–59. [PubMed: 12614607]
18. Torkko JM, et al. Candida tropicalis expresses two mitochondrial 2-enoyl thioester reductases that are able to form both homodimers and heterodimers. J Biol Chem. 2003; 278:41213–41220. [PubMed: 12890667]

19. Miwa GT, Garland WA, Hodshon BJ, Lu AY, Northrop DB. Kinetic isotope effects in cytochrome P-450-catalyzed oxidation reactions. Intermolecular and intramolecular deuterium isotope effects during the N-demethylation of N,N-dimethylphentermine. J Biol Chem. 1980; 255:6049–54. [PubMed: 6771263]
20. Khare D, et al. Structural Basis for Cyclopropanation by a Unique Enoyl-Acyl Carrier Protein Reductase. Structure. 2015; 23:2213–2223. [PubMed: 26526850]
21. Almarsson O, Bruice TC. Evaluation of the Factors Influencing Reactivity and Stereospecificity in Nad(P)H Dependent Dehydrogenase Enzymes. Journal of the American Chemical Society. 1993; 115:2125–2138.
22. Burgner JW, Ray WJ. The Lactate-Dehydrogenase Catalyzed Pyruvate Adduct Reaction - Simultaneous General Acid-Base Catalysis Involving an Enzyme and an External Catalyst. Biochemistry. 1984; 23:3626–3635. [PubMed: 6477888]
23. Benach J, Atrian S, Gonzalez-Duarte R, Ladenstein R. The catalytic reaction and inhibition mechanism of Drosophila alcohol dehydrogenase: Observation of an enzyme-bound NAD-ketone adduct at 1.4 angstrom resolution by X-ray crystallography. Journal of Molecular Biology. 1999; 289:335–355. [PubMed: 10366509]
24. Bull HG, et al. Mechanism-based inhibition of human steroid 5 alpha-reductase by finasteride: Enzyme-catalyzed formation of NADP-dihydrofinasteride, a potent bisubstrate analog inhibitor. Journal of the American Chemical Society. 1996; 118:2359–2365.
25. Maier T, Leibundgut M, Ban N. The crystal structure of a mammalian fatty acid synthase. Science. 2008; 321:1315–1322. [PubMed: 18772430]
26. Kwan DH, Leadlay PF. Mutagenesis of a modular polyketide synthase enoylreductase domain reveals insights into catalysis and stereospecificity. ACS Chem Biol. 2010; 5:829–38. [PubMed: 20666435]
27. Quade N, Huo LJ, Rachid S, Heinz DW, Muller R. Unusual carbon fixation gives rise to diverse polyketide extender units. Nature Chemical Biology. 2012; 8:117–124.
28. Erb TJ, Brecht V, Fuchs G, Muller M, Alber BE. Carboxylation mechanism and stereochemistry of crotonyl-CoA carboxylase/reductase, a carboxylating enoyl-thioester reductase. Proceedings of the National Academy of Sciences of the United States of America. 2009; 106:8871–8876. [PubMed: 19458256]
29. Ames BD, et al. Crystal structure and biochemical studies of the trans-acting polyketide enoyl reductase LovC from lovastatin biosynthesis. Proceedings of the National Academy of Sciences of the United States of America. 2012; 109:11144–11149. [PubMed: 22733743]
30. Erb TJ, et al. Synthesis Of C-5-dicarboxylic acids from C-2-units involving crotonyl-CoA carboxylase/reductase: The ethylmalonyl-CoA pathway. Proceedings of the National Academy of Sciences of the United States of America. 2007; 104:10631–10636. [PubMed: 17548827]
31. Vlasie MD, Banerjee R. When a spectator turns killer: Suicidal electron transfer from cobalamin in methylmalonyl-CoA mutase. Biochemistry. 2004; 43:8410–8417. [PubMed: 15222752]
32. Toney MD. Controlling reaction specificity in pyridoxal phosphate enzymes. Biochimica Et Biophysica Acta-Proteins and Proteomics. 2011; 1814:1407–1418.
33. Toney MD. Reaction specificity in pyridoxal phosphate enzymes. Archives of Biochemistry and Biophysics. 2005; 433:279–287. [PubMed: 15581583]
34. Ghanem M, Murkin AS, Schramm VL. Ribocation transition state capture and rebound in human purine nucleoside phosphorylase. Chem Biol. 2009; 16:971–9. [PubMed: 19778725]
35. Dawson, RMC. Data for biochemical research. Clarendon Press; Oxford: 1986. p. 580xii
36. Kabsch W. Xds. Acta Crystallogr D Biol Crystallogr. 2010; 66:125–32. [PubMed: 20124692]
37. Winn MD, et al. Overview of the CCP4 suite and current developments. Acta Crystallogr D Biol Crystallogr. 2011; 67:235–42. [PubMed: 21460441]
38. Afonine PV, et al. *phenix.model_vs_data*: a high-level tool for the calculation of crystallographic model and data statistics. J Appl Crystallogr. 2010; 43:669–676. [PubMed: 20648263]
39. Murshudov GN, Vagin AA, Dodson EJ. Refinement of macromolecular structures by the maximum-likelihood method. Acta Crystallogr D Biol Crystallogr. 1997; 53:240–55. [PubMed: 15299926]

40. Emsley P, Lohkamp B, Scott WG, Cowtan K. Features and development of Coot. Acta Crystallogr D Biol Crystallogr. 2010; 66:486–501. [PubMed: 20383002]

41. Chen VB, et al. MolProbity: all-atom structure validation for macromolecular crystallography. Acta Crystallogr D Biol Crystallogr. 2010; 66:12–21. [PubMed: 20057044]

Europe PMC Funders Author Manuscripts

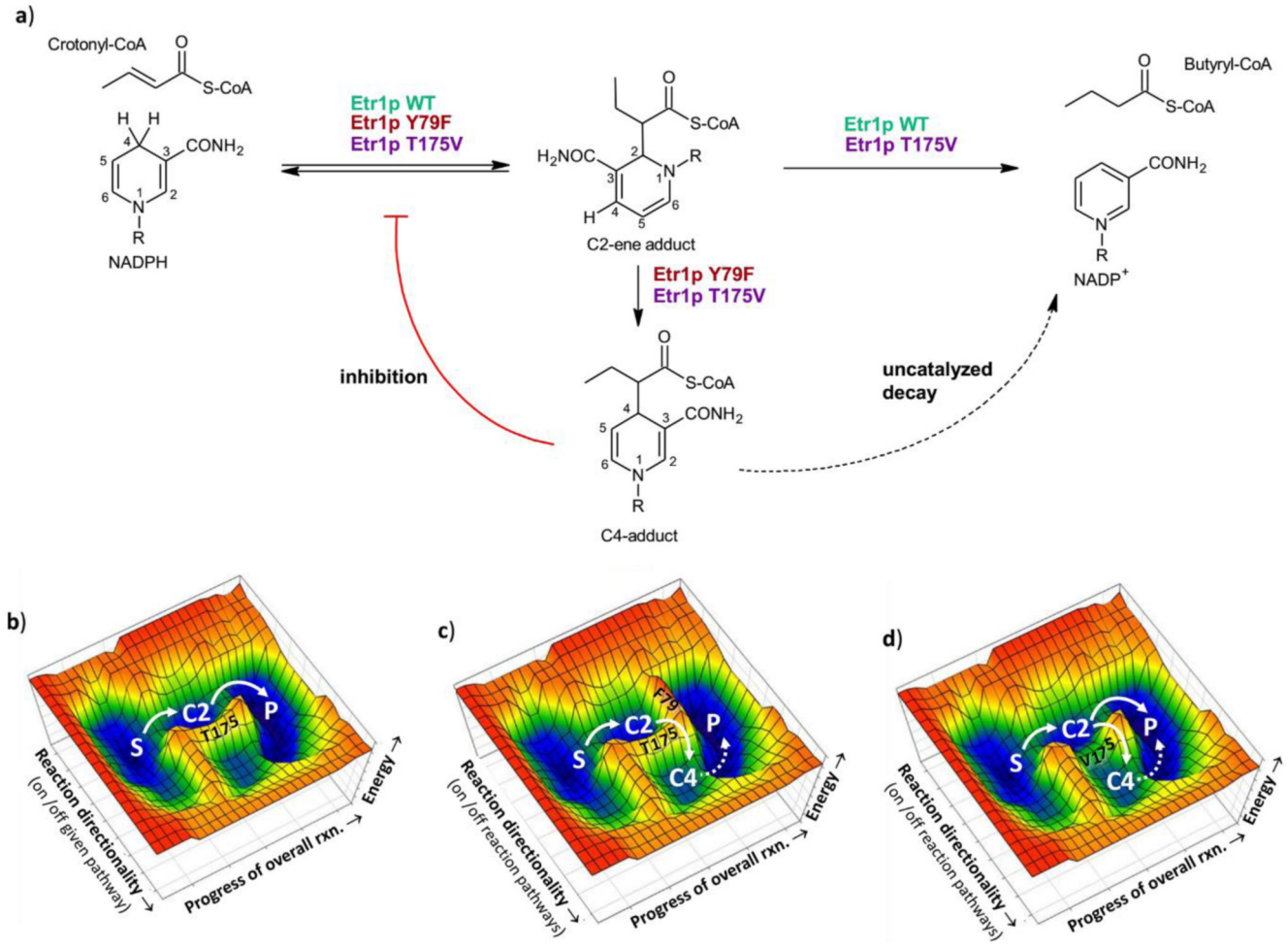

Figure 1. Reaction schemes of Etr1p WT and variants and their effect on a hypothetical catalytic landscape.

a) Reaction scheme of Etr1p WT, Etr1p Y79F and Etr1p T175V. Etr1p WT catalyzes the NADPH-dependent conversion of crotonyl-CoA into butyryl-CoA. Etr1p Y79F converts crotonyl-CoA with NADPH to the C2-ene adduct and subsequently to the C4-adduct. The C4-adduct is a strong inhibitor of Etr1p (red line) and decays slowly in solution (dotted line). Etr1p T175V still catalyzes the NADPH-dependent conversion of crotonyl-CoA into butyryl-CoA, but also formation of the C4-ene adduct, thereby inhibiting itself. **b)** Hypothetical landscape of Etr1p WT catalysis. **c)** Hypothetical landscape of Etr1p Y79F catalysis. Mutation of the proton donor Y79F raises the energetic barrier of the protonation step, causing formation of the C4-ene adduct. **d)** Hypothetical landscape of Etr1p T175V catalysis. Mutation of T175 lowers the energetic barrier to form the C4-adduct leading to C4-adduct accumulation and self-intoxication of the enzyme even though the protonation step in the T175V is still functional. Abbreviations used: S, substrates; P, products; C2, C2-ene adduct; C4, C4-adduct.

Europe PMC Funders Author Manuscripts

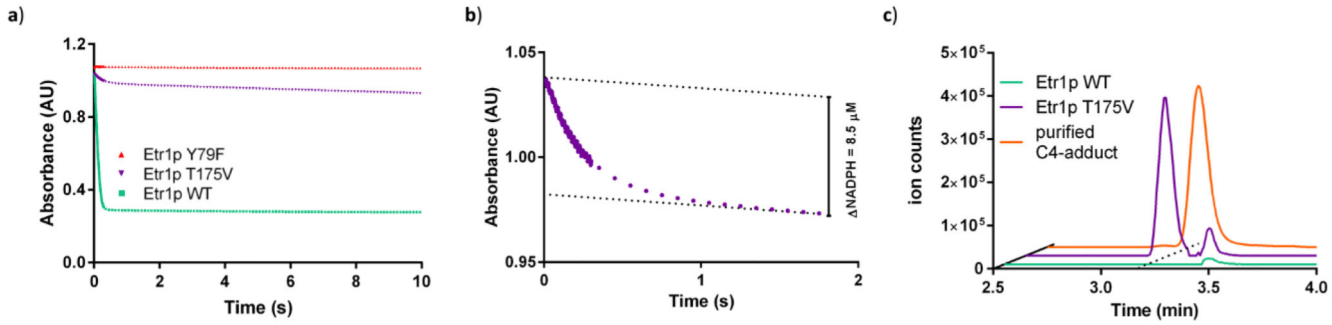

Figure 2. Detailed characterization of the reactions catalyzed by Etr1p WT and variants.

The experiments show that T175V is still active but intoxicates itself rapidly by formation of the C4-adduct. **a)** Stopped flow kinetics of Etr1p WT (green), the proton donor mutant Y79F (orange) and the T175V variant (purple). T175V shows a two phasic behavior. An initial burst-phase that lasts only for 3 turnovers followed by a slow linear phase (see panel **b**). All assays contained 2.5 μM enzyme, 160 μM NADPH and 120 μM crotonyl-CoA in 20 mM Tris-HCl buffer (pH 7.9) with 150 mM NaCl. Data shown are representatives of at least three independent experiments. **b)** Close up of the first 2 seconds of the reaction of Etr1p T175V. After 3 turnovers, the burst phase turns into the linear phase. **c)** UPLC-MS analysis of assays with either Etr1p WT (green) or the T175V variant (purple). The T175V variant shows accumulation of a C4-adduct (compare to authentic C4-adduct standard, orange trace), while the Etr1p WT did not accumulate detectable amounts of the C4-adduct. Data shown are representatives of at least three independent experiments.

Europe PMC Funders Author Manuscripts

Europe PMC Funders Author Manuscripts

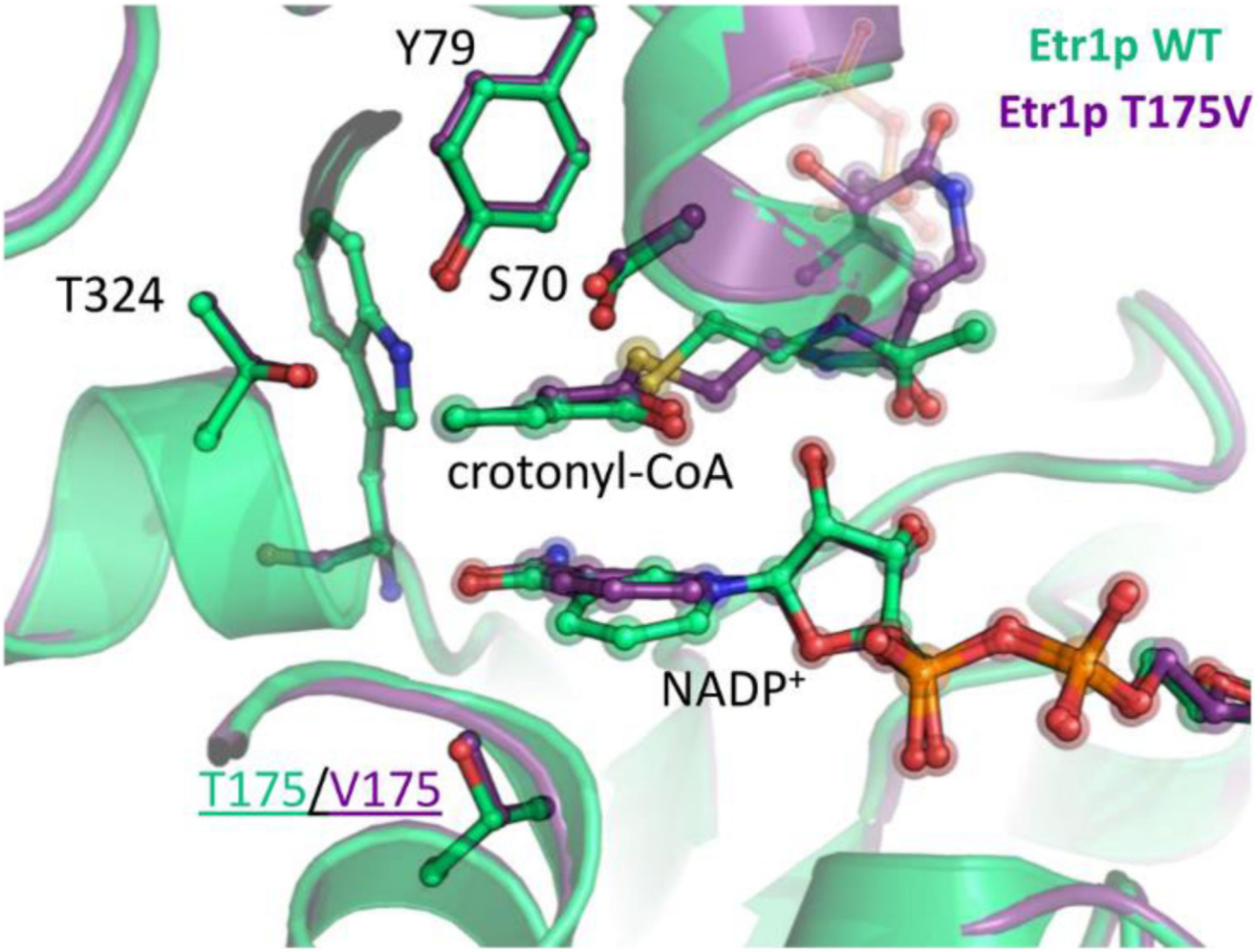

Figure 3. Crystal structure of Etr1p WT and the T175V variant.

Overlay of crystal structures of Etr1p WT and the T175V variant, co-crystallized with $NADP^+$ and soaked with crotonyl-CoA. The structures superimpose with a rmsd of 0.45 Å. The only notable difference near the active site is a slight shift in the nicotinamide ring of $NADP^+$.

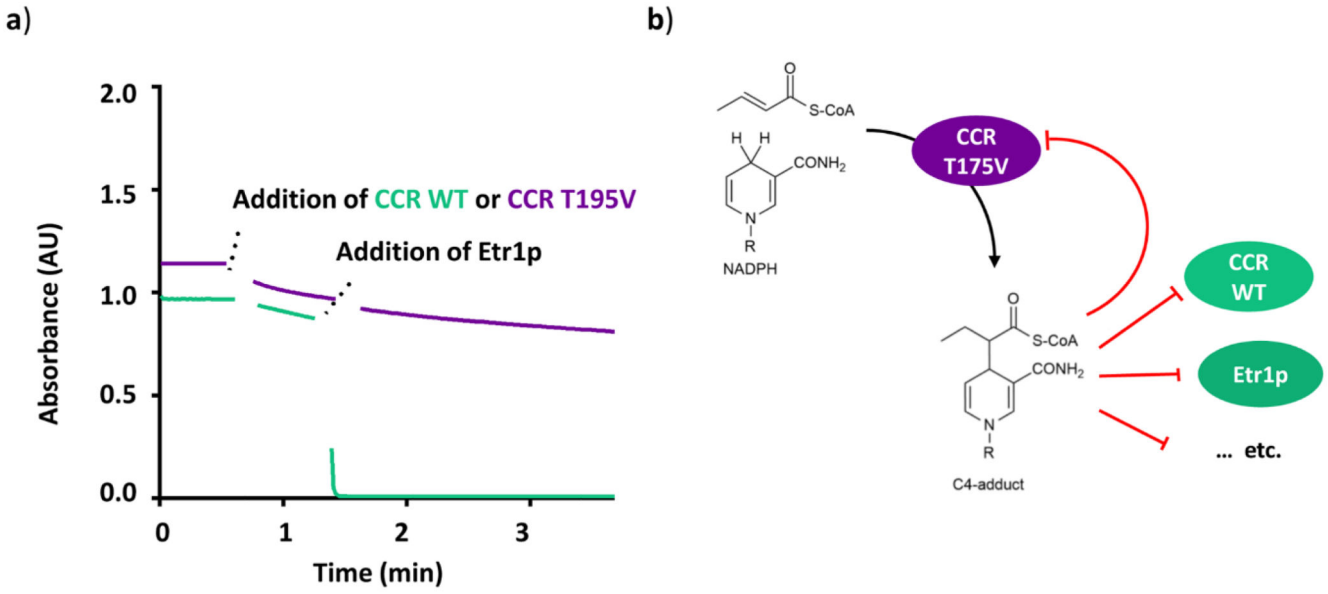

Figure 4. Cross-inhibition between Et1p WT and CCR T195V

a) CCR WT (1.7 μM) was added (after 40 s) to a reaction assay containing NADPH and crotonyl-CoA that was monitored at 340 nm (green trace). After 90 s, Etr1p WT was injected into the mixture, leading to the rapid depletion of NADPH. In an equivalent assay, in which CCR T195V was used instead of CCR WT (purple trace), addition of Etr1p did not cause NADPH consumption, indicating that Etr1p was inhibited. Data shown are representatives of at least three independent experiments. **b)** Model explaining the observed cross-inhibition. CCR T195V forms the C4-adduct during catalysis, which leads to a rapid "self-intoxication" of the enzyme. The C4-adduct is also able to diffuse into other enzyme active sites, to effectively inhibit these enzymes, too. Selection for avoiding C4-adduct formation in NAD(P)H-dependent enzymes thus acts beyond individual enzyme level.

Europe PMC Funders Author Manuscripts